Journal of Interfaces, Thin films, and Low dimensional systems 4 (2) Winter and Spring (2021) 393-403

Effect of vacancy defects on the Josephson current in zigzag graphene narrow strips

Scientific research paper

Somayyeh Zareei[1], Vahid Daadmehr[1,2*], Hossein Hakimi Pajouh[1*], Zahra Faraei[3]

[1]*Department of Physics, Faculty of Physics and Chemistry, Alzahra University, Tehran, Iran*

[2]*Magnet & Superconducting Res. Lab, Department of Physics, Alzahra University, Tehran, Iran*

[3]*Department of Physics, Institute for Advanced Studies in Basic Sciences (IASBS), Zanjan 45137-66731, Iran*

ARTICLE INFO

Article history:
Received 8 October 2021
Revised 16 November 2021
Accepted 19 November 2021
Available online 10 December 2021

Keywords:
Graphene narrow stripe
Josephson current
Vacancy defect
Lattice model

ABSTRACT

We investigate the Josephson current in a superconductor/zigzag graphene narrow strip/superconductor (Sc-ZGNS-Sc) junction with vacancy defects. For this purpose, we extend a recursive Green's function based numerical method to ZGNSs and take into account the effect of vacancies including random single vacancy distributions and also chain-like linear defects. We investigate how the Josephson current is affected by the length and width of the strip and the concentration of the vacancies. We find that the Josephson current exhibits an exponential dependence on the vacancy concentration. The exponent coefficient is a nonlinear function of the length of the lattice and the vacancy concentration. For the width dependence we find a linear relation between the Josephson current and the width of the ZGNS which propose a semi classical treatment of the electron transport in the system. Finally, we study the effect of chain-like linear defects and compare them with randomly distributed single vacancies.

1 Introduction

Since its discovery, graphene, a single atomic layer of carbon atoms in a hexagonal lattice structure, has attracted much research attention, both theoretically and experimentally, due to its unique mechanical, thermal, and electrical properties [1, 2, 3]. The peculiar electronic structure of graphene has become a major cause of enthusiasm among scientists. Linear energy dispersion relation near the discrete Fermi points and chiral nature of charge carriers in graphene has been reported which have caused attractive phenomena [4, 5]. Among the phenomena of graphene, the superconducting proximity effect is one of the most attractive properties from both basic and applied points of view. This phenomena has been studied theoretically [6] and experimentally [7] where good contacts between the superconductor electrodes and graphene have been established while the Josephson current through a superconductor-graphene-superconductor junction has been measured.

In graphene, high carrier mobility at room temperature, and unique electrical properties make them a promising material for a variety of nano-electronics applications [8]. At present, graphene can be synthesized in two ways: namely top-down method and bottom-up method. The top-down approach can involve the structural breakdown of graphite followed by the interlayer separation to produce graphene sheets

*Corresponding authors.
Email address: Daadmehr@alzahra.ac.ir; hhpajouh@Live.com
DOI: 10.22051/jitl.2022.37391.1061

[9] while the bottom-up technique such as chemical vapor deposition, epitaxial growth and total organic synthesis implements carbon molecules as building blocks [10]. In the preparation processes of graphene, it is difficult to avoid defects. Various defects, such as vacancy defects [11, 12, 13], impurity defects [14, 15] and adsorption defects [16, 17], could be introduced. In most cases these unavoidable defects can influence the characteristics of the graphene, such as energy band structure, carrier mobility, thermal and electrical conductivities, electronic transport properties like the Josephson current and so on. On the other hand, the different types of defects could change the topology or the curvature and then change the geometric structure of graphene [18]. Perhaps even more importantly, nearest neighbor carbon atoms to defect rearrange themselves into a variety of different polygons, not only hexagons (pentagons, octagons and so on), to form different structures with lower energy states by changing the bonding geometry around the defect. The vacancy defects, which are a very basic type of defect, are discussed here. A vacancy defect is empty space of a carbon atom located in the inner part or on the edge of graphene, which usually either appears during synthesis process [19, 20], or artificially is produces by techniques like ion and electron irradiation or chemical approaches [12, 13, 21].

The effect of short-range disorder on graphene's conductance has been investigated in [22]. It was illustrated in [23] that the electrical conductance of graphene largely depends on the type and concentration of point defects. Single vacancy low concentrations noticeably do not degrade electron transport. In comparison, double vacancy induces a moderate reduction of 25–34% in graphene. By increasing the concentration of defects, the electrical conductivity can be reduced by a factor of about 2-3 compared to low concentrations. Reference [24] investigates the disordered single-layer graphene Josephson junctions with dimension of $W \gg L$ and shows that if we consider the average current as a function of vacancy concentration, increasing vacancy concentration leads to power-law suppression of the critical current.

Reference [25] shows that the position and concentration of vacancies in graphene nanoribbons affect their transmission spectrum and thus their current-voltage characteristics. Motivated by this, we present in this paper a numerical study of the Josephson current in a graphene strip Josephson junction with different vacancy concentrations.

In our previous work [26], we examined the Josephson current for a graphene strip without vacancy, the results of which were in good agreement with the theoretical and experimental results obtained for graphene. Josephson current in a two dimensional square lattice contacting two superconductors was studied by Furusaki [27]. Generalizing the conventional recursive Green's function technique to superconducting systems, he developed a method to numerically study the DC Josephson current in dirty SNS junctions. The results showed an agreement with the estimations of analytic calculations. Extending this formalism to brick lattices, we study the Josephson effect in a narrow strip of graphene with arbitrary length L and width $W < L$ for zigzag edges. Transfering the hexagonal lattice structure into a brick-like structure conserves the lattice topology [28], which is responsible for the low-energy excitations of the graphene strip. With this method, we investigate the Josephson current in graphene strips with different length and different vacancy concentrations.

The paper is organized as follows. In section 2 we describe our numerical method to calculate the Josephson current using a lattice model which is a basic tool for the numerical study of the effects of vacancy defects. In section 3, results are presented followed by the related discussions. Finally, we end the paper with the main conclusions in section 4.

2 Model and method

The system consists of a graphene nano stripe (GNS) coupled to two conventional s-wave spin-singlet superconductor leads as shown in Figure 1. We proposed a 2D array arranged in a brick-wall lattice. This lattice represents a special case of the honeycomb lattice [28, 29], both of which can be strained into each other through continuous deformation and support two Dirac points in the corners of the 2D Brillouin zone (Fig. 2). By this consideration, our starting point is the tight-binding Hamiltonian on the pristine (without vacancy) Sc-GNS-Sc system, which we include the possibility for different horizontal and vertical nearest neighbors hopping. The full Hamiltonian takes the form:

$$H = -t_h \sum_\sigma \Big(\sum_{j=0}^{n_x}\sum_{k=0}^{n_y}\big(c^\dagger_{j,k,\sigma}c_{j-1,k,\sigma} + c^\dagger_{j-1,k,\sigma}c_{j,k,\sigma}\big)\Big) - t_v \sum_\sigma \Bigg(\sum_{\substack{j=0\\ j\ is\ odd}}^{n_x}\sum_{k=0}^{n_y}\big(c^\dagger_{j,k,\sigma}c_{j,k+1,\sigma} + c^\dagger_{j,k+1,\sigma}c_{j,k,\sigma}\big)\Bigg) - t_v \sum_\sigma \Bigg(\sum_{\substack{j=0\\ j\ is\ even}}^{n_x}\sum_{k=0}^{n_y}\big(c^\dagger_{j,k,\sigma}c_{j,k-1,\sigma} + c^\dagger_{j,k-1,\sigma}c_{j,k,\sigma}\big)\Bigg) + \sum_{j=0}^{n_x}\sum_{k=0}^{n_y}\sum_\sigma \varepsilon_{j,k}c^\dagger_{j,k,\sigma}c_{j,k,\sigma} - \mu\sum_{j=-\infty}^{\infty}\sum_{k=0}^{n_y} c^\dagger_{j,k,\sigma}c_{j,k,\sigma} - \sum_{j=-\infty}^{\infty}\sum_{k=0}^{n_y}\big(\Delta_{j,k}c^\dagger_{j,k,\downarrow}c^\dagger_{j,k,\uparrow} + \Delta^* c_{j,k,\uparrow}c_{j,k,\downarrow}\big), \quad (1)$$

where $c^\dagger_{j,k,\sigma}(c_{j,k,\sigma})$ is a creation (annihilation) operator of an electron on site $\boldsymbol{r} = (j,k)$ with spin $\sigma(=\uparrow \text{or} \downarrow)$. $t_h(t_v)$ is the nearest neighbors hopping matrix element in the horizontal (vertical) direction and μ is the chemical potential. Here, j and k are the cell counters in horizontal and vertical directions, respectively. The number of places in the transverse direction is as $n_y + 1$ and in the horizontal direction is as $n_x + 1$. So, the length of the normal region (L) is $n_x a_0$ and its width (W) is $n_y a_0$, where a_0 is the lattice constant. The system has a strip geometry that confines the graphene electrons in a (large) length and a finite (small) width, so, $n_y \ll n_x$. The order parameter Δ_{jk} is assumed to be constant in the left (Δ_L for $j < 0$) and right ($\Delta_R e^{i\phi}$ for $j > n_x$ that ϕ is the phase difference between the left and right superconductors) superconductors and zero in the middle region ($0 < j_x < n_x$).

Imposing the current conservation law, one finds the Josephson current through the interface between the jth and (j+1)th cells, as follows [27, 30]:

$$I = -\frac{iet}{\beta\hbar}\sum_\sigma\sum_{k=0}^{n_y} < c^\dagger_{j.k.\sigma}c_{j+1,k,\sigma} - c^\dagger_{j+1,k,\sigma}c_{j,k,\sigma} > = \frac{iet}{\beta\hbar}\sum_{\omega_n}\sum_{k=0}^{n_y} Tr\,[G_{\omega_n}(j,k;j+1,k) - G_{\omega_n}(j+1,k;j,k)], \quad (2)$$

where <…> means the thermal average and $\beta = 1/K_B T$ with k_B is the Boltzman constant, and T is the temperature. $G_{\omega_n}(j,k;j',k')$ is the Nambu Green's Function (2×2 matrix) with the Matsubara frequency $\omega_n = \pi K_B T(2n+1)$ (n= 0, ±1, ±2, ...) which in each region satisfies the equation of motion [27]:

$$\begin{pmatrix} \mathbf{i\omega_n - H_{j,k}} & -\Delta_{\mathbf{j,k}} \\ -\Delta^*_{\mathbf{j,k}} & \mathbf{i\omega_n + H^*_{j,k}} \end{pmatrix}\mathbf{G_{\omega_n}(j,k;j',k')} = \boldsymbol{\delta_{j,j}\delta_{k,k'}}. \quad (3)$$

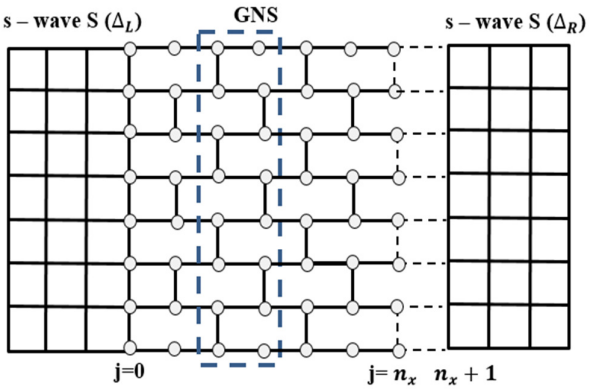

Figure 1. Schematic illustration of the Sc-ZGNS-Sc junction which the order parameter in the left (right) superconductor is as $\Delta_L(\Delta_R e^{i\phi})$ and in the middle normal region is zero. The unit cell is indicated with blue dashed lines. White empty circles are the Carbon atoms in the brick-wall lattice of the graphene strip.

It is possible to explicitly calculate the Green's function of three separate regions. Substituting the connected Green's function in Eq. (2) will compute the Josephson current. The procedure has been outlined in detail in Ref [27] and also appendix A. We will here only outline the essentials in order to illustrate how we extend this numerical method to a brick-wall lattice and also how we include the vacancies.

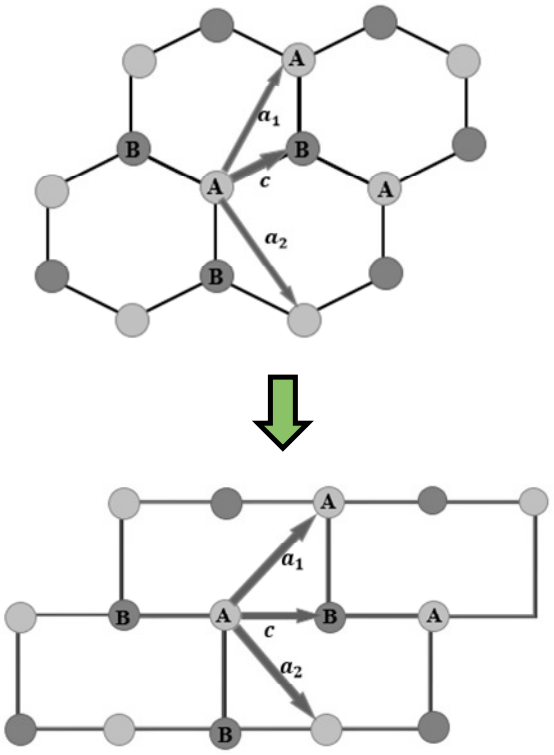

Figure 2. Schematic structure of honeycomb lattice and brick-wall lattice. The sub lattices A and B in the unit cell and the basis vector c is represented in both lattice. The primitive unit cell is defined by the primitive vectors $\boldsymbol{a_1 and\ a_2}$.

For the normal region we can think of unit cells as shown in Figure 1 which the jth cell consists of the sites (j,k) with $k = 0, \dots, ny$. Attaching the cells to the left superconductor one by one and using the cursive Green function method [31], Green's function of the middle region is:

$$G_{\omega_n}(j,k;j',k') = [i\omega_n\delta_{k,k'}I - H_j(k,k') - H_t G_{\omega_n}(j-1,k;j-1,k')H_t]^{-1}, \quad (4)$$

where $H_j(k,k') = \begin{pmatrix} \mathrm{H}_0 & 0 \\ 0 & -\mathrm{H}_0^* \end{pmatrix}$ is the BdG Hamiltonian of the jth cell with

$\mathrm{H}_0 = -\mathrm{t_v}\left(\delta_{\mathrm{k,k'-1}} + \delta_{\mathrm{k,k'+1}}\right) + \left(\varepsilon_{\mathrm{j,k}} - \mu\right)\delta_{\mathrm{k,k'}}$ and $\mathrm{H}_t = -t_h \begin{pmatrix} 1 & 0 \\ 0 & -1 \end{pmatrix}$ being the hopping between two neighboring cells. The effect of a vacancy is taken into account through the change in the hopping elements t_h and t_v. We consider two distinct approaches. In the first approach, removing of a single carbon atom is equivalent to disappearing of one vertical and two horizontal hopping elements. This attitude is perfected by forming a weak horizontal bond between the left and right atoms of the vacancy which is shown schematically in Figure 3 . The new bond has a modified hopping matrix element which is relative to t_h as $t_h e^{-\ell/a}$ with ℓ being the length of the new bond while a is the lattice constant. Accidental placement of two or more holes in a horizontal row corresponds to a longer bond length, resulting in a smaller hopping coefficient.

Our next approach is based on the fact that in graphene, the formation of divacancies (DVs) are energetically more favorable than two separate vacancies (about 8 eV compared to 15 eV) [32, 33]. They can be created either by the coalescence of two single vacancies or by removing two neighboring atoms. The presence of such thermodynamically preferred DVs which causes a defective lattice to be cohesive are very common in reported experimental graphene samples [34, 12]. Removing an atom from the lattice causes the geometry around the vacancy to change so that all the dangling bonds are saturated as the lattice relaxes to a lower energy state. This lattice relaxation leads to non-hexagonal bond geometries and the formation of non-hexagonal rings, causing slight disturbances in the bond lengths around the vacancy (Fig. 9).

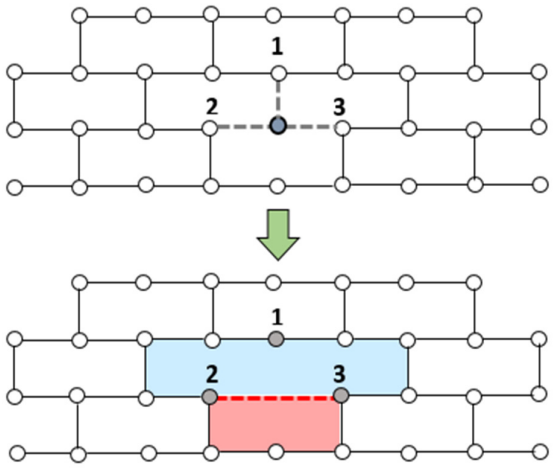

Figure 3. Removing of a single carbon atom of GNS lattice. In the first approach, one vertical and two horizontal hopping elements disappear. In the second approach, removing an atom from the lattice causes the geometry around the vacancy to change so that non-hexagonal rings are formed.

3 Results and discussion

We start with a pristine lattice by considering different lengths from n_x =10 to 120 and different widths from n_y = 10 to 50. The chemical potential in the normal region is set to be $\mu_n = 0.001\, eV$ and for the superconducting regions, we assume $\mu_s = 1.7\, eV$. This means that the Fermi wave vector in the S regions is large compared to the normal region and so we allowed to adopt a step function model for Δ at the interface [35].The temperature is $T = 3.13\, K$ (which is in the range of temperatures related to reference [36]) and we consider three different widths. The results are plotted in Fig. 4a for three values of the width (n_y/n_x = 0.1, 0.2, 0.5).

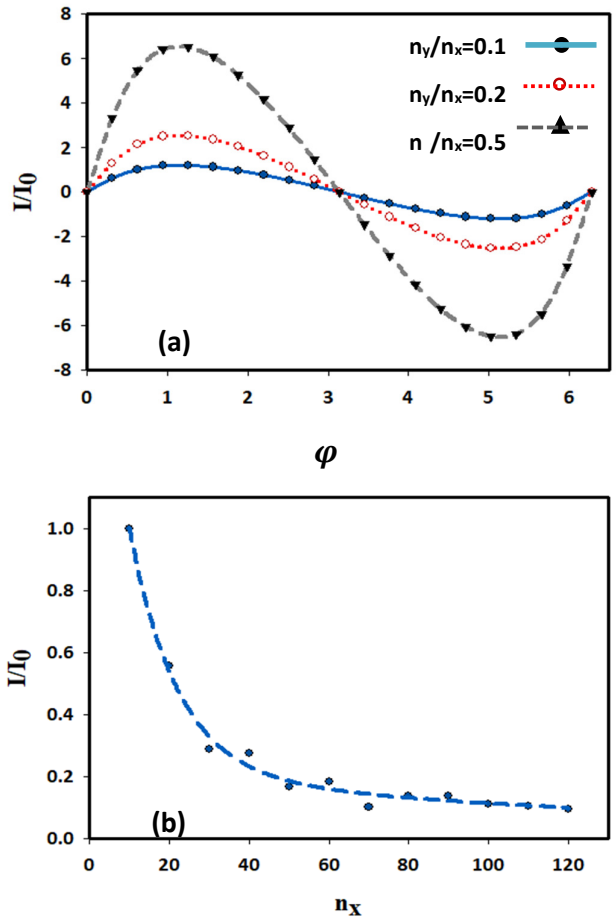

Figure 4. Normalized Josephson current density of Sc-pristine ZGNS-Sc junction in terms of (a) phase difference of superconductors with different ratio of width to the length of the ZGNS region and (b) the length of the graphene strip, with fixed $n_y = 10$. The current is scaled to I_0 that is the current of pristine ZGNS with the width (the length) of ny=10 (n_x=10) and = $\frac{\pi}{2}$.

The phase dependence of the Josephson current which deviates from the traditional sinusoidal form, is in good agreement with the predicted theoretical [37] and experimental [36] results. This feature is due to the low density of conduction channels near the Dirac point and exponentially-decaying evanescent states.

This relationship is maintained when the junction length L is shorter than the superconducting coherence length ξ, where $\xi = \hbar v_F/\Delta_0$, to allow coherent transport of superconducting pairs. It should be noted that the largest phase drop we can put over the whole structure is π. Qualitatively, Fig. 4a is in agreement with the numerical results shown in [37]. Reference [36] experimentally measures CPR of a graphene Josephson junction and shows that the CPR is skewed with respect to the commonly observed sinusoidal behavior. As seen, whatever the ratio of the stripe width to the length is greater, the maximum current is also greater, which is the same as the result obtained from Figure 8, in which it was shown that current has linear dependence on the width. Figure 4b shows the length dependence of the current in the short junction region. As can be seen, it decays exponentially with increasing length. In reference [37] it is shown that in low doping limit, $\mu \approx 0$, functionally, the I vs.L dependence form is also close to the traditional Ginzburg-Landau Ce^{-L/ξ_N} form.

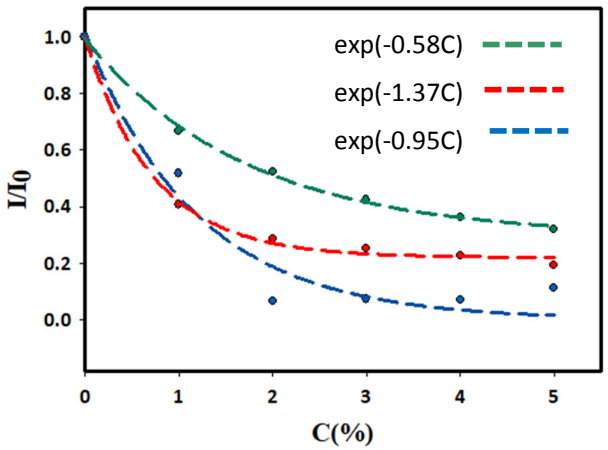

Figure 5. Normalized Josephson current vs. the concentration of vacancies for three different lattice lengths of ZGNS (green dashed line for n_x=10, red dashed line for n_x=50 and blue dashed line for n_x=100).

Now we turn to the vacancy defects. We study how the presence of various distributions of vacancies influences the Josephson current of our system. Figure 5, shows the Josephson current in terms of vacancies concentrations for three different lattice lengths ($n_x = 10, 50, 100$). The vertical axes is normalized to the Josephson current of the perfect sample (I_0). To achieve a satisfactory statistical behavior, we averaged on about 300 different random configurations of vacancy's distributions to obtain each point in these curves. Vacancy concentration (C) which is the ratio of the number of vacancies to the number of all carbon atoms, varies from 0% to 5%. Each single vacancy corresponds to formation of a two adjacent nine-member and five-member neighboring rings (Figure 3). As one can see in Figure 5, the first result is that the presence of vacancies leads to the reduction of the Josephson current. Here the dashed lines show the exponential fits and represent a decay coefficient for each vacancy concentration (γ). As seen, γ is a function of the graphene strip.

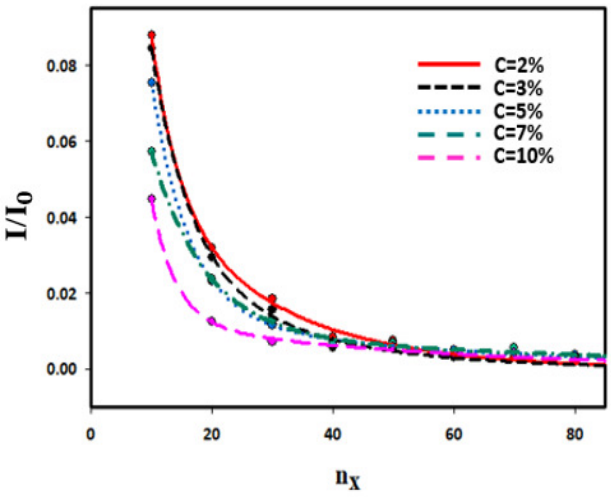

Figure 6. Normalized Josephson current density vs. length of ZGNS for three different concentrations of vacancies (C=2%, 3%, 5%, 7% and 10%). The dashed lines show the exponential fitting.

The longer ZGNS (n_x=100) drops faster than those of shorter ones (n_x=10, 50) and approaches to zero. Figure 6 shows this feature from a different viewpoint. The Josephson current through the defective ZGNS is plotted as a function of its length at different vacancy concentrations, C=2%, 3%, 5%, 7% and 10%. Each curve defines a localization length (ξ) exponent for a specific concentration which is not only a function of the system size but it depends on the vacancy concentration. The Josephson current is caused by Andreev bound states that characterize quasi-classical paths that start at one of the superconducting leads and return to the starting point after reaching the opposite superconductor. These Andreev paths constitute the supercurrent channels and the total phase change in each Andreev loop which is related to the mean free path of charge carriers between two superconductors that have to be an integer multiple of 2π. Increasing the vacancy concentration reduces the average free path of the electron, thus reduces the number of supercurrent channels and consequently the Josephson current. Therefore, it is not far-fetched that the dependence of the Josephson current on the length and concentration of vacancies is similar to the dependence of the conduction on these parameters [38].

When a carbon atom is removed from the graphene stripe lattice, the probability of the carrier hopping from this vacancy is exponentially reduced. The results show that the same exponential reduction is reflected in Josephson's current.

Moreover, increasing the concentration of vacancies, quantum mechanically, corresponds to a greater correlation between them. This increase in correlation manifests itself in the enlargement of the exponent's coefficient α. To better illustrate this result, in Fig. 7, we present the log plot of normalized Josephson current in terms of n_x. Table 1 shows the numerical values of the localization length (which is the inverse of α). As can be seen, the localization length increases with increasing concentration of vacancies.

Table 1. Comparison of the exponent coefficient $\boldsymbol{\alpha}$ and localization length $\boldsymbol{\xi}$ for different vacancy concentrations.

The vacancy concentration	2%	3%	5%	7%
The Coefficient (α)	0.025	0.023	0.012	0.0084
Localization length (nm)	40	43.48	83.33	119.05

We also discuss the dependence of the Josephson current on the width of ZGNS (Figure 8). Our results show that the Josephson current increases linearly with increasing the width of ZGNS. It seems that we are dealing with a quasi-classical phenomenon. If we

consider each of the longitudinal lines of the ZGNS lattice as a transport channel that connects the left and right superconductors, the increase in lattice width corresponds to a linear increase in the number of these channels.

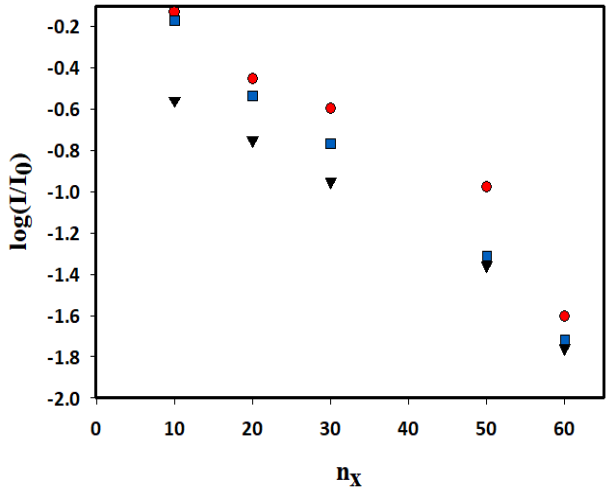

Figure 7. Plot of log (I/I_0) as function of length of ZGNS for three different concentrations of vacancy: C=2% (red circle), C=5% (blue square) and C=7% (black triangle)).

This linear increasing is also observed in the normal state resistance of ZGNR [39, 40]. At very narrow widths, which are not the subject of our discussion, the effect of borders is noticeable, and this classical view does not work. But in the mesoscopic dimension of perfect graphene strips, electron transport is quasi-ballistic and is analyzed using the Landau-Büttiker formalism [41, 42]. Although the presence of vacancies changes the lattice linkages, but the linear behavior of the current with respect to the width remains true.

Now we consider divacancies which strongly disrupt the uniformity of C–C bonds around these defects in graphene lattice. When all the dangling bonds are saturated and no dangling bonds remain, in the place of these defects, two pentagons and one octagon appear instead of the previous four hexagons. In addition, the rotation of the created bonds also leads to the creation of various other polygons. Figure 9 shows schematically three types of these polygons in the graphene honeycomb lattice and their equivalents in our brick-wall lattice. Multiple DVs form an extended line of defects (ELDs). These defects can be fabricated by controlled focused electron beam irradiation [43] or single atom resolution aberration corrected transmission electron microscopy [44].

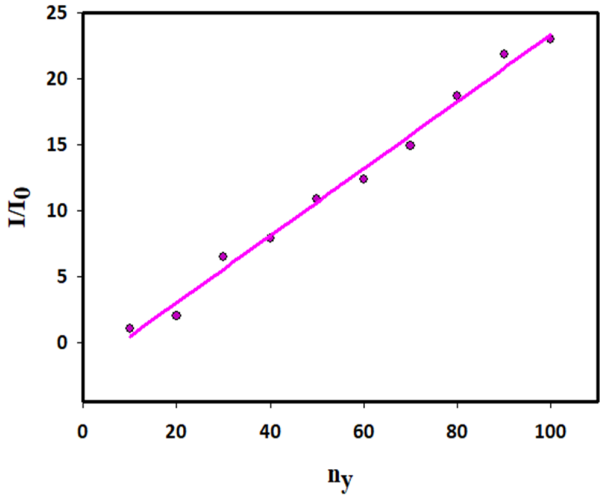

Figure 8. Normalized Josephson current vs. width of ZGNS for vacancy concentration C=5% and $n_x = 10$. The current of ZGNSs is scaled to I0 that is the current of pristine ZGNS with the width of ny=10.

To find the relation between Josephson current and the formation of different ELDs, we have compared the Josephson current in three different ELDs with simple combination of single vacancies which place next to each other. As shown in Fig. 9, in each ELD, two neighboring atoms are removed which results in an eight-member ring in the lattice. In the first horizontal 5-8-5 ELD (Fig. 9a), the eight-member rings are on a horizontal line but in the other two vertical 5-8-5 ELD (Fig. 9b), and 4-8 ELD (Fig. 9c), the rings are all on the same vertical line. The difference between the last two is that in the vertical 5-8-5 ELD, there is a vertical C-C bond between two neighboring DV rings, but in the 4-8 ELD there is no space between the DV rings. It can be seen that the number of vacancies in each ELD is equal to the number of 8-member rings formed.

Table 2 illustrates the comparison of the Josephson current in these three ELDs and the correspondence randomly distributed SVs. The lattice is considered as n_x=60 and n_y=40 with 6 vacancies that the concentrations of the vacancies in all four configurations are the same, but the Josephson currents are very different from each other.

Using the physics, we described earlier, this difference is understandable. In the horizontal ELD, the removing of 6 carbon atom results in disconnection of only one transport channel, but in vertical ELDs, three transport channels are disjointed. Hence, we expect to have a larger Josephson current in the horizontal loop Josephson current in the horizontal loop. To compare vertical ELDs, it is necessary to pay attention to the fact that in 4-8 ELD, the vacancies are closer to each other, so the correlation between them is stronger and as a result the localization length is shorter and the current reduction due to this configuration will be greater. Calculating the current in a lattice of six holes randomly distributed in the lattice shows that the Josephson current in this case is less than the horizontal loop but more than vertical loop.

Table 2. Comparison of Josephson current of 6 vacancy defects in ZGNR lattice with n_x=60 and n_y=40 for 4 different configurations.

Defect type	Configuration	Josephson current (I/I_0)
Single vacancy	5-9	0.82
Double vacancy	horizontal 5-8-5	0.94
	vertical 5-8-5	0.3
	5-8-4-8-5	0.15

(a)

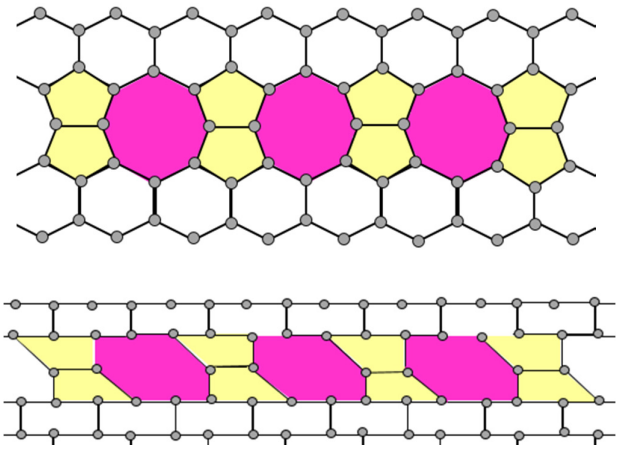

(b)

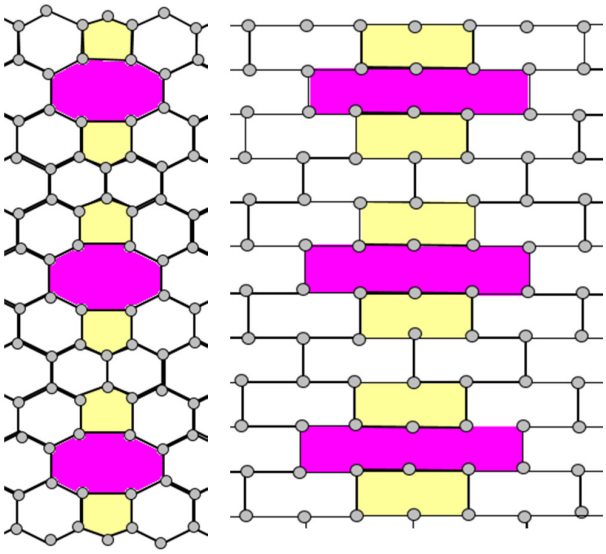

(c)

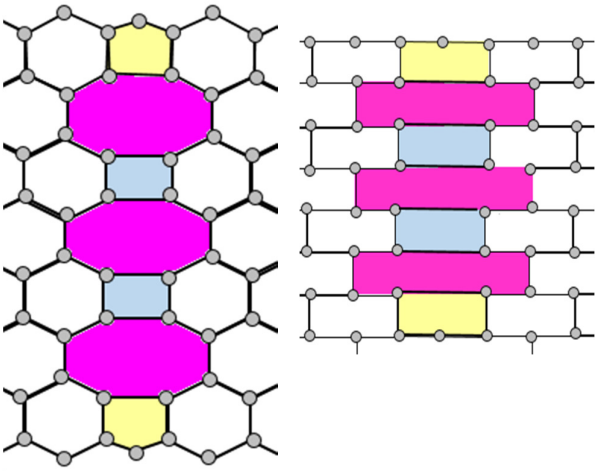

In this work, we investigate the effect of vacancy defects on the Josephson current of a Sc-ZGNS-Sc hetero structure. We found that the behavior of the Josephson current is a combination of semi classical and quantum treatments. When the width of the ZGNS increases, the semi classical part reveals as a linear increase of the Josephson current in terms the width. It seems that adding each row of lattice corresponds to adding a transport line and consequently a linear increase in Josephson current. This behavior is independent of the concentration of vacancies. However, the dependence of Josephson current to the length arises quantum mechanically from the

exponentially decaying of the hopping matrix elements and also the correlation of vacancy places. These features are confirmed in the study of the Josephson current of linear chain of divacancies. Finally, we considered the role of linear chain of divacancies which is usually formed in real samples.

Acknowledgments

S. Z. and V. D. wish to thank for financial support of the vice chancellor research and technology of Alzahra university.

Appendix A

As given in reference [27], the Green's function can be calculated separately for each region (the left superconductor, the normal region, the right superconductor). Then, the Green function of the connected system is obtained which is needed in calculating the Josephson current. By starting from the left superconductor ($j \le 0$) which at first is not connected to the normal region (Figure 1) the Green function in the edge of the left superconductor is given by:

$$G_{\omega_n}(0,k;0,k') = \sum_{=1}^{n_{y+1}} \frac{e^{ip^{+}_{m,L}}}{t_h \Omega_{n,L}(n_y+2)} \sin[q \ (k+1)] \sin[q \ (k'+1)] \times \begin{pmatrix} -\Omega_{n,L}-\omega_n & i\Delta_L \\ i\Delta_L & \Omega_{n,L}-\omega_n \end{pmatrix} - \sum_{=1}^{n_{y+1}} \frac{e^{-ip^{-}_{m,L}}}{t_h \Omega_{n,L}(n_y+2)} \sin[q \ (k+1)] \ \sin[q \ (k'+1)] \times \begin{pmatrix} \Omega_{n,L}-\omega_n & i\Delta_L \\ i\Delta_L & -\Omega_{n,L}-\omega_n \end{pmatrix}, \quad (5)$$

Where $\Omega_{n,L(R)} = \sqrt{\omega_n^2 + \Delta^2_{L(R)}}$, $q_m = m\pi/(n_y+2)$, and $p^{\pm}_{m,L(R)} = \arccos[-(\mu + 2t_h \cos q_m \pm \Omega_{n,L(R)})/2t_h]$.

Next we separate the normal region into cells in such a way that the jth cell consists of the site (j, k) (k=0…, n_y) and attach the cells to the left superconductor one by one, see Figure 1. Then we obtain the Green's function in normal region that is given in model and method section.

Finally we attach the right superconductor to the semi-infinite SN system. To this end we need the Green function for the right superconductor:

$$G_{\omega_n}(n_x+1,k;n_x+1,k') = \sum_{=1}^{n_{y+1}} \frac{e^{ip^{+}_{m,R}}}{t_h \Omega_{n,R}(n_y+2)} \sin[q \ (k+1)] \sin[q \ (k'+1)] \times \begin{pmatrix} -\Omega_{n,R}-\omega_n & i\Delta_R e^{i\varphi} \\ i\Delta_R e^{-i\varphi} & \Omega_{n,R}-\omega_n \end{pmatrix} - \sum_{=1}^{n_{y+1}} \frac{e^{-ip^{-}_{m,R}}}{t_h \Omega_{n,R}(n_y+2)} \sin[q \ (k+1)] \sin[q \ (k'+1)] \times \begin{pmatrix} \Omega_{n,R}-\omega_n & i\Delta_R e^{i\varphi} \\ i\Delta_R e^{-i\varphi} & -\Omega_{n,R}-\omega_n \end{pmatrix}. \quad (6)$$

Then the Green function of the connected system which we need in calculating the Josephson current is obtained from the following two equations:

$$G_{\omega_n}(n_x,k;n_x+1,k') = \sum_{k'=0}^{n_y} \{[G_{\omega_n}(n_x,k;n_x,k')]^{-1} - H' G_{\omega_n}(n_x+1,k;n_x+1,k') H'\}^{-1} \times H' \times G_{\omega_n}(n_x+1,k;n_x+1,k'), \quad (7)$$

$$G_{\omega_n}(n_x+1,k;n_x,k') = \sum_{k'=0}^{n_y} G_{\omega_n}(n_x+1,k;n_x+1,k') \times H' \{[G_{\omega_n}(n_x,k;n_x,k')]^{-1} - H' G_{\omega_n}(n_x+1,k;n_x+1,k') H'\}^{-1}. \quad (8)$$

The Josephson current is calculated from Eqs. (2), (7), and (8).

References

[1] A.K. Geim, "Graphene: Status and Prospects." Science, **324** (2009) 1530.

[2] Marks, M.C. Hersam, "Carbon nanomaterials for electronics, optoelectronics, photovoltaics, and sensing." Chemical Society Reviews, **42** (2013) 2824.

[3] Y. Zhu , et al, "Graphene and Graphene Oxide: Synthesis, Properties, and Applications." Advanced Materials, **22** (2010) 3906.

[4] A.K. Geim, K.S. Novoselov, "The rise of graphene." Nature Materials, **6** (2007) 183.

[5] A.H. Castro Neto, F. Guinea, N.M. R. Peres, K.S. Novoselov, and A.K. Geim, "The electronic properties of graphene." Reviews of Modern Physics, **81** (2009) 109.

[6] C.W. J.Beenakker, M. Titov , "Josephson effect in ballistic graphene." Physical Review B, **74** (2006) 041401.

[7] C. Ojeda-Aristizabal, M. Ferrier, S. Guéron, and H. Bouchiat, "Tuning the proximity effect in a superconductor-graphene-superconductor junction." Physical Review B, **79 (**2009) 165436.

[8] M. Wilson, "Electrons in atomically thin carbon sheets behave like massless particles." Physics Today, **59** (2006)21.

[9] V. Eswaraiah, et al, "Top down method for synthesis of highly conducting graphene by exfoliation of graphite oxide using focused solar radiation." Journal of Materials Chemistry, **21** (2011) 6800.

[10] L. Tang, et al, "Bottom-up synthesis of large-scale graphene oxide nanosheets/" Journal of Materials Chemistry, **22** (2012) 5676.

[11] Y. Kim, J. Ihm, E.Yoon, G.D. Lee, "Dynamics and stability of divacancy defects in graphene." Physical Review B, **84** (2011) 075445.

[12] J. Kotakoski, A.V. Krasheninnikov, U. Kaiser, and J.C. Meyer, "From Point Defects in Graphene to Two-Dimensional Amorphous Carbon." Physical Review Letters, **106** (2011) 105505.

[13] A. Hashimoto, K. Suenaga, A. Gloter, K. Urita, S. Iijima, "Direct evidence for atomic defects in graphene layers." Nature, **430** (2004) 870.

[14] K. Brenner, R. Murali, "In situ doping of graphene by exfoliation in a nitrogen ambient." Applied Physics Letters, **98** (2011) 13115.

[15] C. Zhang, L. Fu, N. Liu, M. Liu, Y. Wang, Z. Liu, "Synthesis of Nitrogen□Doped Graphene Using Embedded Carbon and Nitrogen Sources." Advanced Materials, **23 (**2011) 1020.

[16] L. Li, S. Reich, J. Robertson, "Defect energies of graphite: Density-functional calculations." Physical Review B, **72** (2005) 184109.

[17] C. Ataca, E. Akturk, H. Şahin, S. Ciraci, "Adsorption of carbon adatoms to graphene and its nanoribbons." Journal of Applied Physics, **109** (2011) 013704.

[18] M. Terrones, A.R. Botello-Méndez, J. Campos-Delgado, F. López-Urías, Y.I. Vega-Cantú, F.J. Rodríguez-Macías, A.L. Elias, E. Munoz-Sandoval, A.G. Cano-Marquez, J. Charlier, "Graphene and graphite nanoribbons: Morphology, properties, synthesis, defects and applications." Nano Today, **5** (2010) 351.

[19] P.T. Araujo, M. Terrones, M.S. Dresselhaus, "Defects and impurities in graphene-like materials." Materials Today, **15** (2012) 98.

[20] C.Ö. Girit, et al, "Graphene at the Edge: Stability and Dynamics." Science, **323** (2009) 1705.

[21] M.M. Ugeda, I. Brihuega, F. Guinea, J.M. Gómez-Rodríguez, "Missing Atom as a Source of Carbon Magnetism." Physical Review Letters, **104** (2010) 096804.

[22] Y. Wang,Y. Wu, "Disorder enhanced conductance in graphene." Physica B, **478** (2015) 84.

[23] L. Nanshu, Z. Si, Z. Jijun, "Electrical Conductance of Graphene with Point Defects." Acta Physico-Chimica Sinica, **35** (2018) 1142.

[24] W.A. Mu˜noz, L. Covaci and F.M. Peeters, "Disordered graphene Josephson junctions." Physical Review B, **91** (2015) 054506.

[25] M. Gokhan Sensoy, "The influence of vacancy-induced local strain on the transport properties in armchair and zigzag graphene nanoribbons."

Materials Research Express, **6** (2019) 045057.

[26] S. Zareei,V. Daadmehr, H. Hakimipajouh, Z. Faraei, "Josephson current for a Graphene nanoribbon using a lattice model. Interfaces, Thin films, and Low dimensional systems, **2** (2019)113.

[27] A. Furusaki, "DC Josephson effect in dirty SNS junctions: Numerical study." Physica B: Condensed Matter, **203** (1994) 214.

[28] W. Hou, J.M. Chen, "Hidden symmetry and protection of Dirac points on the honeycomb lattice." Scientific Reports, **5** (2014) 17571.

[29] K. Wakabayashi, M. Fujita, H. Ajiki and M. Sigrist, "Electronic and magnetic properties of nanographite ribbons." Physical Review B, **59** (1999) 8271.

[30] Y. Asano, "Numerical method for dc Josephson current between d-wave superconductors," Physical Review B, **63** (2001) 052512.

[31] M.P. López Sancho, J.M. Rubio, "Quick iterative scheme for the calculation of transfer matrices: application to Mo (100)." Journal of Physics F: Metal Physics, **14** (1984) 1205.

[32] A.V. Krasheninnikov, P.O. Lehtinen, A.S. Foster, R.M. Nieminen, "Bending th vacancy energetics and migration in graphite and carbon nanotubes." Chemical Physics Letter, **418** (2006) 1205.

[33] A.A. El-Barbary, R.H. Telling, C.P. Ewels, M.I. Heggie, P.R. Briddon, "Structure and energetics of the vacancy in graphite." Physical Review B, **68** (2003) 144107.

[34] F. Banhart, J. Kotakoski, A.V. Krasheninnikov, "Structural Defects in Graphene." ACS Nano, **5** (2011) 26.

[35] C.W.J. Beenakker, "Specular Andreev Reflection in Graphene." Physical Review Letters, **97** (2006) 067007.

[36] G. Nanda, et al,, "Current-Phase Relation of Ballistic Graphene Josephson Junctions." Nano Letters, **17** (2017) 3396.

[37] A.M. Black-Schaffer and S. Doniach, "Self-consistent solution for proximity effect and Josephson current in ballistic graphene SNS Josephson junctions." Physical Review B, **78** (2008) 024504.

[38] effect on the electronic transport of zigzag graphene nanoribbon using recursive Green's function." Computational Materials Science, **101** (2015) 156.

[39] Z. Chen, Y. Lin, M.J. Rooks, P. Avouris, "Graphene Nano-Ribbon Electronics." Physica E, **40** (2007) 228.

[40] Z. Xiao, C. Durkan, "Unravelling the electrical properties of epitaxial Graphene nanoribbons." Advanced Materials Interfaces, **6** (2019) 1801794.

[41] M. time: Effective area in magnetically induced interference." Physical Review B, **36** (1987) 6255.

[42] C. Durkan, Current at the nanoscale: An introduction to nanoelectronics, second edition, World Scientific Publishing Company (2013).

[43] J.H. Warner, G.Do Lee, K. within Extended Arm Chair Defects in Graphene." ACS Nano, **7** (2013) 9860.

[44] A.W. Robertson, G. Allen, "Partial dislocations in graphene and their atomic level migration dynamics." Nano letters, **15** (2015) 5950.